Sustainable Cities and Society 89 (2023) 104374

Contents lists available at ScienceDirect

Sustainable Cities and Society

journal homepage: www.elsevier.com/locate/scs

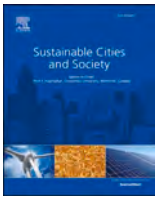

Relationship between urban spatial form and seasonal land surface temperature under different grid scales

Yang Chen [a], Jun Yang [a,b,c,*], Wenbo Yu [b], Jiayi Ren [b], Xiangming Xiao [d], Jianhong Cecilia Xia [e]

[a] Urban Climate and Human Settlements Research' Lab, Jangho Architecture College, Northeastern University, Shenyang 110169, China
[b] School of Humanities and Law, Northeastern University, Shenyang 110169, China
[c] Human Settlements Research Center, Liaoning Normal University, Dalian 116029, China
[d] Department of Microbiology and Plant Biology, Center for Earth Observation and Modeling, University of Oklahoma, Norman, OK 73019, USA
[e] School of Earth and Planetary Sciences (EPS), Curtin University, Perth 65630, Australia

ARTICLE INFO

Keywords:
Urban spatial form
Land surface temperature
Grid scale
XGBoost
Xi'an City

ABSTRACT

The urban heat island (UHI) effect is intensifying with increasing urbanization. As an important representation of the UHI effect and the urban thermal environment, it is critical to investigate the importance of evaluating urban spatial form (USF) indicators on land surface temperature (LST) to alleviate urban thermal environment problems. Therefore, in this study, we evaluated the importance of USF indicators from three perspectives: landscape pattern, building morphology, and social development, on LST at 10 grid scales in the main area of Xi'an City, using the XGBoost model. The results showed that: (1) LST was similar in spring and autumn, but significantly lower in winter. The distribution of high-temperature areas in the four seasons has its own characteristics, but the low-temperature areas are mainly distributed in the water bodies and parks in the north and south of the middle of the study area, which are less affected by the seasons. (2) Mean architecture height (MAH) is a seasonal stable factor with a cooling effect. The relationship between patch density (PD), landscape shape index (LSI), Shannon's diversity index (SHDI), contagion index (CONTAG), people density (POD), floor area ratio (FAR) and LST varies with seasons. The correlation between building density (BD) and LST is complex. (3) The degree of influence of the USF indicators on seasonal LST could be ranked in the following order: building morphology > landscape pattern > social development. (4) The appropriate size to study the relationship between USF and seasonal LST is 60 m. The highest contribution of USF to LST is building morphology, three indicators affect 43%–55% of LST. The findings of this study provide useful information for urban land-use planning and building layout, to mitigate the UHI effect.

1. Introduction

Rapid population growth and urban sprawl during urbanization have resulted in the replacement of a large amount of natural land cover in urban areas with artificial impermeable surfaces, resulting in an imbalance of surface energy exchange and a continuous increase in land surface temperature (LST) in urban built-up areas (X. Li et al., 2017; Li et al., 2020; Zhang and Sun, 2019). Therefore, the temperature in urban areas is higher than in peripheral suburban areas, and this phenomenon is known as the urban heat island (UHI) effect (Howard, 2012; Mandal et al., 2021; Oke et al., 2017). Against the backdrop of current global warming and frequent extreme weather, urban thermal environmental problems are becoming increasingly notable, not only exposing urban residents to constant high temperatures but also having serious negative impacts on certain aspects of social life, such as public health, air quality, and the ecological environment (Aghamohammadi et al., 2021; Y. Lu et al., 2021; He, Wang, Zhu, & Qi, 2022). These circumstances have required quantitative research to characterize the urban thermal environment and to detect the spatial distribution and influencing factors of LST, an important parameter of the change in the UHI effect. This is the key approach to achieving the goals of combating climate change, mitigating the UHI effect, and developing sustainable human settlements (Shi et al., 2019; Sobstyl et al., 2018). Besides climate warming being a direct driver of the UHI effect, various characteristics of urban areas that have developed over the long-term development, such as the urban spatial form (USF), can also affect the intensity of UHI (Taleghani

* Corresponding author.
E-mail address: yangjun8@mail.neu.edu.cn (J. Yang).

https://doi.org/10.1016/j.scs.2022.104374
Received 16 October 2022; Received in revised form 7 December 2022; Accepted 21 December 2022
Available online 24 December 2022

et al., 2015; Zhou and Chen, 2018). Studies have shown a dynamic correlation between USF and LST (Coseo and Larsen, 2014; Zhou et al., 2017). Therefore, exploring the seasonal differences and scale effects of the impact of USF on LST can help governments and urban planners find a balance between urban form planning and urban thermal environment quality control. This is critical to reducing human settlement health risks, mitigating the UHI effect, and ensuring sustainable urban development (J. Yang et al., 2017; Yang et al., 2019; He et al., 2022).

USFs cover numerous aspects, such as regional topography, land use and coverage, and landscape diversity, along with architectural form and its spatial organization (Dan et al., 2022; J. Guo et al., 2020; Huang et al., 2021; Li and Li, 2021). These aspects reflect the spatial configuration of urban functions and regional distribution of human activities; thus, USFs affect the intensity of the UHI effect (Liu et al., 2021). Scholars have conducted some research on the relationship between USFs and LST (Sharifi, 2019). Most studies on USF and LST focus on various combined morphological elements, and explore the spatiotemporal heterogeneity of USF's impact on LST distribution in different research units (Wang et al., 2021; Yang et al., 2020, 2021a).

Although the spatiotemporal relationship between USF and UHI has been quantified, the seasonal variation of multidimensionality indicators in quantitative research on USF and LST has often been ignored. As a broad and comprehensive concept, there is no unified standard for USF measurement (Liu et al., 2017), and there are differences in the measurement indicators selected on different spatial observation scales (Esch et al., 2014; Taubenböck et al., 2019). Liang et al. selected eight indicators from the three categories of scale, geometry, and vegetation to quantify the spatial form of the urban agglomeration scale (Liang et al., 2020). Tsai defined a set of variables to quantitatively characterize urban forms on the metropolitan scale from four aspects: scale, intensity, density, and centrality (Tsai, 2005). Yang et al. used the floor area ratio (FAR), land use coefficient (PR), absolute roughness (Ra), average aspect ratio (λc), and sky view factor (SVF) indicators to characterize the USF on the community scale (Yang et al., 2021b). Although these studies have selected a variety of indicators on different scales to quantify the relationship between USF and LST, they focus more on the two-dimensional (2D) characteristics of cities, while ignoring their 3D shape. With the continuous expansion of cities and buildings in horizontal and vertical directions, scholars have focused on the relationship between the 3D urban form and LST. Researchers have widely used building height, BD, FAR, etc. as 3D USF indicators, and have shown a significant correlation between these indicators and LST (Huang and Wang, 2019; Li et al., 2021). Because of this, more scholars began to contemplate the impact of 2D and 3D USF on LST and have made some meaningful exploration. However, there are few studies on the seasonal differences in the relationship between USF and LST.

Few existing studies have focused on the scale dependence of the relationship between USF and LST. However, some recent studies have focused on the relationship between a single aspect of USF and LST (A. Guo et al., 2020a). For example, Estoque et al. showed the densities of the impervious surface and the green space have a strong correlation with LST, and the optimal spatial scale for that study was 210 m (Estoque et al., 2017). Li and Hu found that 240 m was the best scale to investigate the marginal effect of building form indexes on LST (Li and Hu, 2022). Song et al. indicated that 660 m and 720 m are the most suitable scales for exploring the relationship between landscape composition indicators and LST (Song et al., 2014). However, these studies focused only on single aspects of USFs, such as landscape pattern or architectural form. Becasue of this, the scale response relationship between multifaceted USF indicators and LST still needs to be investigated.

The choice of model to explore the relationship between USF and LST is also a key issue. To quantitatively explore how different USF affect LST, the most common approach includes regression analysis methods (Morabito et al., 2016), of which ordinary least squares (OLS) regression has been the most widely used. The global OLS model can reflect the global fitting relationship between the USF and the LST in the study area. However, because traditional regression analysis such as OLS regression begins with the assumption of observational independence, the interrelationships between different spatial units are downplayed, and the spatial dependence of the data is neglected (Li et al., 2010). To address these problems and be able to comprehensively measure thermal interaction on the urban surface space, the spatial lag model and the spatial error model are widely used. These spatial regression models add spatial relationships based on traditional regression models, while combining attribute data with spatial locations through spatial relationships and consider the correlation between the spatial observations of geographic data (A. Guo et al., 2020b; Kim et al., 2016; Yang and Jin, 2010). Furthermore, to better explain the non-stationarity of the regression relationship caused by the spatial heterogeneity and spatial correlation between USF and LST, scholars have developed the geographically weighted regression (GWR) model (Fotheringham et al., 2017; Gao et al., 2020; W. Li et al., 2017). GWR and its improved models combine the spatial weight matrix to fill the defect of the traditional regression model, in which it cannot reflect local changes in regression coefficients (Liu et al., 2019; Stone et al., 2012). Furthermore, machine learning models represented by random forest regression have been used to examine the quantitative relationship between USF and LST, due to the challenges posed by the nonlinear relationship between certain USF indicators and LST as well as the general overfitting of the above model (Equere et al., 2020; Sun et al., 2019a). However, few existing studies have used the XGBoost (eXtreme Gradient Boost) regression model, an extreme gradient boosting tree algorithm that combines supervised learning with integrated learning (Chen and Guestrin, 2016). Compared with traditional machine learning models, XGBoost has multiple advantages, such as greater accuracy, greater flexibility, avoidance of overfitting, and better handling of missing values, which can be used to study the relationship between USF indicators and LST.

To supplement gaps in existing research, we selected the main area of Xi'an City as the study area, quantitatively characterized USFs from multiple aspects, and explored the relationship between USF and LST. Specifically, our study focused specifically on the following aspects: (1) investigation of the spatial heterogeneity of seasonal LST; (2) quantitative characterization of USF from multiple dimensions, including urban landscape pattern, building morphology, and social development; (3) maximization of relationship fitting between USF indicators and LST using the XGBoost model; and (4) analysis of the degree of response of the above relationship to the grid scale.

2. Materials and methods

2.1. Study area

Xi'an City is the capital of Shanxi Province, the core city of the Xi'an metropolitan area. It has a warm temperate semi-humid continental monsoon climate, with four distinct seasons and a large temperature difference. The annual average temperature is 13.0–13.7 ℃, whereas the average temperature in summer is as high as 27.7 ℃. As the largest city in northwest China, Xi'an City has experienced rapid urbanization development and rapid expansion of the urban area with the strategic support of the western development of China. According to public data of the Xi'an Statistical Yearbook, the urban built-up area of Xi'an in 2019 is 729.14 km^2, over twice the 342 km^2 in 2010, and the urban resident population is 1,020.35 million in 2019. In the rapid expansion of urban scale, the increase in population and buildings has brought great environmental pressure to Xi'an, resulting in environmental problems such as the UHI effect, typical in large cities in China. Given its climate and socioeconomic characteristics, Xi'an City was an ideal city for this study. We focused on the urban core areas of Xi'an City, including the Xincheng, Beilin, Lianhu, Baqiao, Yanta, and Weiyang districts. The specific range is shown in Fig. 1.

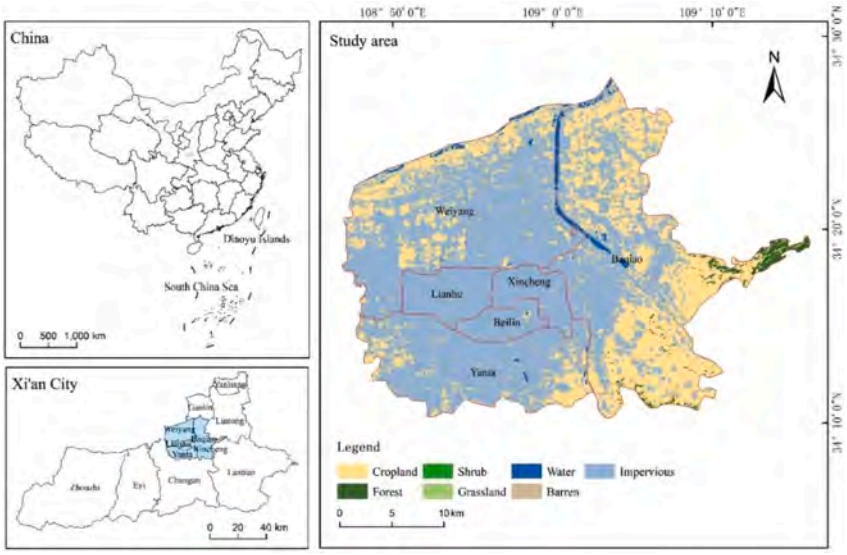

Fig. 1. Location of the study area.

2.2. Data sources

The data used in this study included mainly Landsat8 remote sensing images, and land use, building outline, population density, nighttime light, and administrative boundary data. The data sources and descriptions are shown in Table 1. The strip number of Landsat8 images that covered the study area was 127, and the row number was 36. The Landsat8 images, obtained from the United States Geological Survey (USGS), were used to invert LST. The land use data were obtained from the European Space Agency and used to calculate the landscape pattern index. The building data, obtained from the AutoNavi map open platform, was used to calculate building morphological parameters. Nighttime light data was obtained from the National Oceanic and Atmospheric Administration (NOAA) and was used for nighttime light intensity calculations. The population density data adopted the world population density map released by Worldpop, which is the most accurate and reliable long-term population density data.

2.3. Methods

In this study, we retrieved the study area's LST, selected nine USF indicators, and used the XGBoost model to study the spatial distribution characteristics of LST and the relationship between LST and USF at different grid scales. First, based on the thermal infrared band of the Landsat8 image data, the radiation transfer equation (RTE) method was used to retrieve the seasonal LST. Subsequently, from the perspectives of landscape pattern, building morphology, and social development, nine indicators of the USF were selected. Furthermore, the study area was divided into different grids to explore the spatial distribution of the LST and various USF indicators on different grid scales. Based on the spatial statistical analysis of LST data, the side length of the grid should be an integral multiple of 30 m. However, the 30 m grid is too small and the amount of calculation data is too large. Therefore, because of the pixel size of the data and previous research, the 60 m grid was selected as the smallest grid for spatial statistical analysis (Song et al., 2014). In this study, 10 grid sizes were selected for analysis, including 60 × 60 m, 120 × 120 m, 180 × 180 m, 240 × 240 m, 300 × 300 m, 360 × 360 m, 420 × 420 m, 480 × 480 m, 540 × 540 m, 600 × 600 m. Finally, the XGBoost model was used to explore the relationship between LST and various USF explanatory variables. The specific process of the experiment is shown in Fig. 2.

Note: OLI, operational land imager; LST, land surface temperature; USF, urban spatial form.

Table 1
Data sources and descriptions

Data type	Time	Spatial resolution	Source
Landsat8 OLI_TIRS	2019	30 m	USGS(https://earthexplorer.usgs.gov/)
Land use	2019	10 m	CLCD(http://doi.org/10.5281/zenodo.4417809)
Building data	2018	—	AMAP(https://lbs.amap.com/)
VIIR-NPP	2019	500 m	NOAA(https://www.ngdc.noaa.gov/)
Population density	2019	100 m	Worldpop(https://www.worldpop.org/)
Administrative boundary	2019	—	National Geomatics Center of China

Note: USGS, the United States Geological Survey; CLCD, China's Land-Use/Cover Datasets; VIIR-NPP: Visible Infrared Imaging Radiometer Suite of the Suomi National Polar-Orbiting Partnership; NOAA, the National Oceanic and Atmospheric Administration.

2.3.1. LST retrieval

In this study, we selected Landsat 8 TIRS images with daytime cloudiness below 5% in four seasons and used the RTE to retrieve the LST (Sobrino et al., 2004). Specific image information is shown in Table 2. The basic principle of this method is to simulate the impact of the atmosphere on the surface thermal radiation and then subtract this impact from the total thermal radiation observed by the sensor to obtain the surface thermal radiation intensity, which is then converted into the corresponding surface temperature. The formula could be expressed as follows:

$$L_\lambda = [\varepsilon B(T_S) + (1-\varepsilon)L\downarrow]\tau + L\uparrow \quad (1)$$

In the formula, L_λ represents the thermal infrared radiance value of wavelength λ received by the satellite sensor, ε is the surface specific emissivity, T_S is the surface physical temperature (K), and $B(T_S)$ is the black body radiance. The atmospheric transmittance τ, the atmospheric downlink radiance $L\downarrow$, and the atmospheric uplink radiance $L\uparrow$ for the infrared band are three basic parameters that can be calculated according to the atmospheric correction parameter calculator proposed by (Barsi et al., 2003) on the National Aeronautics and Space Administration website by entering the imaging time and the central latitude and longitude of the image. The calculation results of the parameters τ, $L\downarrow$, and $L\uparrow$ are shown in Table 2.

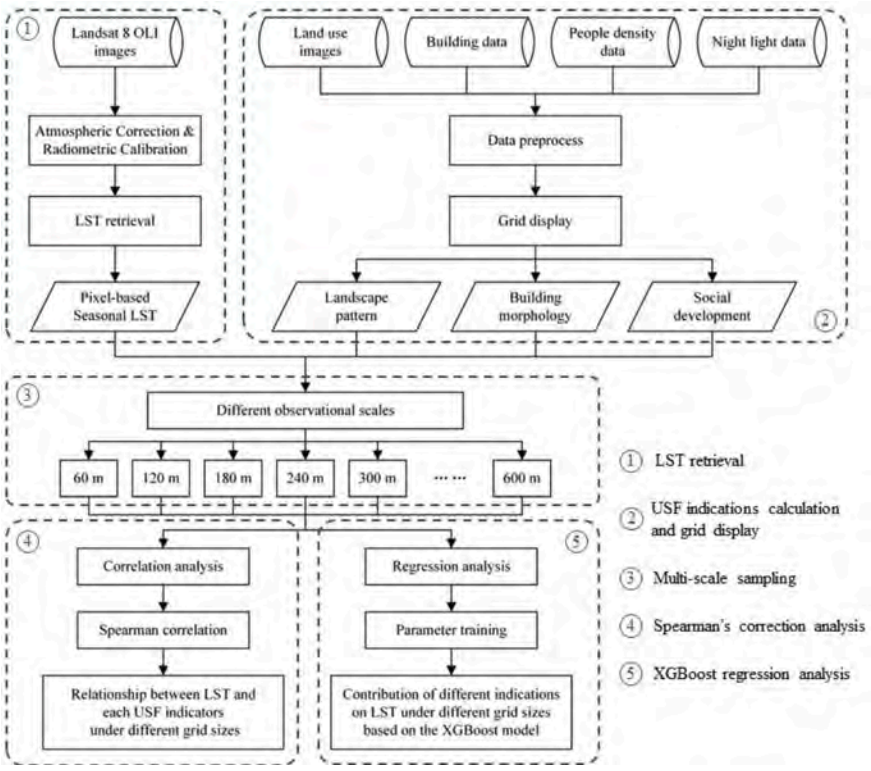

Fig. 2. Methodology of the study.

Table 2
Specific information of Landsat 8 imagery and atmospheric correction parameters of LST retrieval

Season	Image ID	Time	$L\downarrow$	$L\uparrow$	τ
Spring	LC81190312019265LGN00	2019/04/07	0.87	1.50	0.88
Summer	LC81270362019241LGN00	2019/08/29	0.86	1.48	0.89
Autumn	LC81200382019256LGN00	2019/09/30	1.83	1.48	0.76
Winter	LC81190432019265LGN00	2019/01/17	0.14	0.25	0.97

According to the inverse function of Planck's Law, the black body radiance $B(T_S)$ calculated as:

$$B(T_S) = \frac{[L_\lambda - L\uparrow - \tau(1-\varepsilon)L\downarrow]}{\tau\varepsilon} \quad (2)$$

Then, the real surface temperature T_S can be calculated as:

$$T_s = \frac{K_2}{\ln\left(\frac{K_1}{B(Ts)} + 1\right)} \quad (3)$$

where K_1 and K_2 are constant. For Landsat-8 OLI/TIRS images, $K_1 = 774.89 W{*}m^{-2}{*}sr^{-1}\mu m^{-1}$, K_2=1,321.08K.

2.3.2. Indicator selection

A city is a complex dynamic system, and its spatial structure and form are affected by social, economic, policy-related and other factors. Therefore, when exploring the relationship between USF and LST, USF should be quantified from multiple perspectives (Qu et al., 2015; Zhao et al., 2016). Moreover, previous studies have shown that the impact of USF indicators on LST varies with scale, with landscape pattern, building height, building density and other factors having different thermal effects at different spatial scales (Chun and Guldmann, 2014; Guo et al., 2015). Because of this, nine USF indicators were selected to explore their relationship with LST at different grid scales, in terms of landscape pattern, building morphology, and social development. The formulas and specific connotations of each indicator are shown in Table 3.

As an important component of urban spatial pattern characterization, four landscape pattern indices were selected for this study, including patch density (PD), landscape shape index (LSI), Shannon's diversity index (SHDI), and contagion index (CONTAG), which can effectively represent the ecological environment formed by the interaction of natural and human factors in a certain region. PD and LSI are landscape unit characteristic indices that reflect the fragmentation degree of landscape segmentation and the shape complexity of landscape patches, respectively. The SHDI is a landscape heterogeneity index that reflects the homogeneity and complexity of the distribution of different patch types in a landscape within a region. CONTAG is a spatial relationship index of landscape elements that describes the degree of aggregation or extension of patch types. The results of the landscape pattern index were calculated using FRAGSTATS 4.3 software. The building morphology is another important aspect of USF, and the building distribution pattern notably affects the spatial distribution of LST (Sun et al., 2020). Therefore, to characterize the USF, this study selected three indicators—average mean architecture height (MAH), building density (BD), and floor area ratio (FAR) to explore their impact on LST. In addition, because USFs and social development are closely related, we used population density and nighttime light to reflect the level of regional social economic development. Population density has the characteristics of being detached from the specific indicators of economic and social entities, and can effectively represent the level of social development, whereas nighttime lighting is an indicator of the convergence of economic space.

2.3.3. Correction analysis

To explore the impact of various USF indicators on LST, we studied the correlation between these indicators and LST in four seasons on 10 grid scales. Correlation analysis refers to the analysis of two or more correlated variable elements to measure the degree of correlation between variable factors. The most common forms are Pearson's simple, Spearman's, and Kendall's correlations. After inspection, the data

Table 3
Description of urban spatial form factors

Type	Variables (abbreviated)	Formula	Description
Landscape index	Patch density (PD)	$PD=\frac{n_i}{S}$	Different landscape patch densities in the analytical unit.
	Landscape shape index (LSI)	$LSI=\frac{E}{minE}$	The degree of landscape shape complexity.
	Shannon's diversity index (SHDI)	$SHDI=-\sum_{i=1}^{m}P_i\times\ln(P_i)$	Across all patch types, the sum of the proportion of each patch type multiplied by each proportion.
	Contagion index (CONTAG)	$CONTAG=\left[1+\frac{\sum_{i=1}^{m}\sum_{k=1}^{m}\left[(P_i)\left(\frac{g_{ik}}{\sum_{k=1}^{m}g_{ik}}\right)\right]\left[\ln(P_i)\left(\frac{g_{ik}}{\sum_{k=1}^{m}g_{ik}}\right)\right]}{2\ln(m)}\right](100)$	Describe the extent of aggregation or extension of each patch types in the landscape.
Building Form	Mean architecture height (MAH)	$MAH=\frac{\sum_{i=1}^{n}H_i}{n}$	Mean building height in the analytical unit.
	Building density (BD)	$BD=\frac{A_i}{A}$	The density of building in the analytical unit.
	Floor Area Ratio (FAR)	$FAR=\frac{\sum_{i=1}^{n}(c\times F)}{A}$	The ratio between the total building area and total land area.
Social development	People density (POD)	$POD=\frac{P_n}{A}$	Average people intensity in the analytical unit.
	Nighttime light (NL)	——	Average night light intensity in the analytical unit.

Note: n_i, total area of each landscape elements; S, total area of all landscapes; E, total length of edge in a landscape in terms of number of cell surfaces; P_i, proportion of the landscape occupied by patch type-i; m, total number of patch types in the landscape; g_{ik}, number of adjacent type-i and type-k plaques; H_i, height of each building; n, number of buildings; A_i, building area within each analytical unit; A, area within each analytical unit; c, number of floors; F, floor area of the building; P_n, number of people.

structure of each indicator in this study did not conform to the normal distribution; therefore, the Spearman's correlation coefficient was selected.

2.3.4. Regression analysis

LST is not determined by a single USF parameter, but results from a combination of factors. Therefore, based on correlation analysis between USF indicators and LST, a regression model needs to be used to further demonstrate the degree of correlation of quantitative changes between variables. This study used the XGBoost model to measure the importance of each indicator to LST. Compared with the traditional boosted tree algorithm, this method has better execution speed and model performance, and has the advantages of high efficiency, flexibility, and portability (Fan et al., 2018). XGBoost is a framework for joint decision making using multiple correlated regression trees, a regression tree input sample is correlated with the training and prediction of the previous regression tree, improving model performance and reduces the final variance of the model (Sun et al., 2019b).

In this study, the average gain was used to evaluate the importance of each indicator when the node was split. The higher the metric value, the more important the indicator for generating predictions. The model was used in the following two steps. In the first step, each USF indicator was considered an independent variable, and the average LST of each grid was the dependent variable. The second step was to calculate the importance of each USF indicator for LST. To further optimize the regression model, we used the grid search method based on tenfold cross-validation proposed by Chang, and the GridSearchCV function was used for parameter optimization (Chang and Lin, 2011). The parameters specifically adjusted for this study are shown in Table 4.

Table 4
Model parameters for XGBoost.

Parameters	Description	Ranges
eta	Represents the learning effect of the model. By reducing the weights at each step, the robustness of the model can be improved.	[0,1]
gamma	Gamma refers to the minimum loss function drop value required for node splitting to decide whether the node splits.	[0, ∞]
max_depth	The maximum depth of each tree, is used to stop learning in time to avoid overfitting caused by too deep trees.	[0, ∞]
min_child_weight	The sum of the minimum weights of leaf nodes, is used to end the split of leaf nodes, and generally represents the minimum number of samples required to build a model.	[0, ∞]
colsample_bytree	This parameter is used to control the proportion of features randomly sampled for each tree.	(0,1]
colsample_bylevel	This parameter is used to control the proportion of the sampling of the number of columns for per split of each level of the tree.	(0,1]
subsample	This parameter refers to the proportion of random sample samples that generate each tree, preventing overfitting or underfitting.	(0,1]
lambda	L2 regularization term for the weights.	—
alpha	L1 regularization term for the weights.	—
seed	The seed of random numbers, used to reproduce the results of random data, and can also be used to adjust parameters.	—

3. Results

3.1. Seasonal variation of LST spatial patterns

Yu et al. used the surface radiation budget network to compare the following three methods for LST retrieval using TIRS images: the RTE method, the single channel algorithm, and the split window algorithm (Yu et al., 2014). The RTE method was proven to have higher inversion accuracy than the other two methods with a root mean square error of less than 1 K.

The spatial distribution of LST of the four seasons in the study area is shown in Fig. 3. The LSTs for the main city of Xi'an in the spring, summer, autumn, and winter seasons ranged from 19.47–43.14°C, 23.40–50.97°C, 19.54–42.52°C, and -1.76–13.34°C, respectively; the standard deviations were 2.45, 2.85, 1.93 and 1.77, respectively. The results showed the LST was similar in spring and autumn, but was significantly higher in summer and lower in winter. This result follows

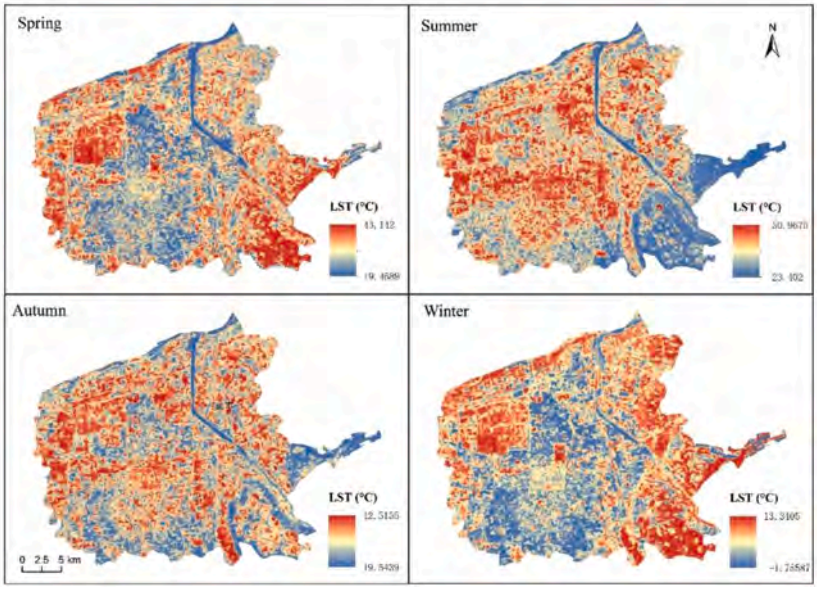

Fig. 3. Spatial distribution of seasonal land surface temperature (LST) in the study area.

the climatic characteristics of Xi'an City—it has four distinct seasons and large temperature difference.

Fig. 3 shows that the spatial distribution of LST in spring and winter was similar. The high- temperature areas were mainly distributed in the southwest of Weiyang, the southeast of Baqiao, and the west of Yanta districts, and scattered high-temperature areas were also distributed in other areas. The LST distributions in summer and autumn showed different laws. The Lianhu, Xincheng, Beilin, Weiyang, northern Yanta, and northwestern Baqiao districts had higher LST than other studied districts in summer and autumn. However, the high-temperature areas in the Lianhu, Xincheng, and Beilin districts in the middle of the study area were more concentrated in summer than in autumn. The LST in the north and south of the central part of the study area is low, mainly because there are water bodies and parks distributed here, and the temperature is less affected by the seasons.

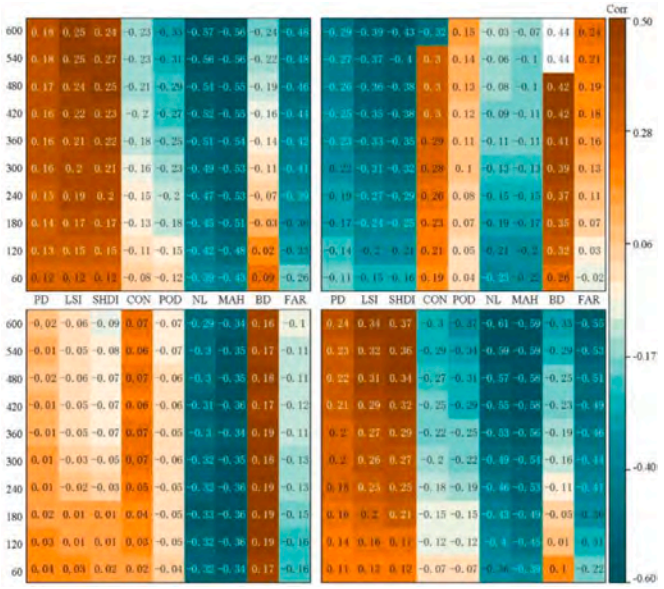

Fig. 4. Correlation between urban spatial form (USF) indicators and land surface temperature (LST)

3.2. Correlation analyses between LST and USF factors

The results of the Spearman's correlation analysis are shown in Fig. 4. The correlation between each indicator and LST was significant at least at the level of 0.05. PD, LSI, and SHDI in the landscape pattern showed consistent regularity. Their relationship with LST showed a positive correlation in spring and winter, a negative correlation in summer, and the positive and negative relationships in autumn changed with the grid scale. However, the relationship between CONTAG and LST showed the opposite rule to the rest of the landscape pattern indicators. Overall, the relationship between the landscape pattern and LST was more obvious in spring, summer and winter than in autumn.

In terms of social development indicators, POD and LST showed a negative correlation in spring, autumn, and winter and a positive correlation in summer; however, the correlation in autumn was low. The correlation coefficient increased with increasing grid scale. NL and LST were negatively correlated in all four seasons; their correlation increased with the increase in the grid scale in spring and winter, decreased with the increase in the grid scale in summer, and remained between the scales in autumn.

Finally, for building morphology indicators, MAH showed the same regularity as NL. BD and LST showed a complex correlation. Spring and autumn were bounded by a 120 m grid. When the grid scale was less than 120 m, BD was positively correlated with LST; otherwise, it was negatively correlated, and the correlation increased with increasing grid scale. BD and LST showed a significant positive correlation in summer and autumn, and BD showed the strongest correlation with LST in summer. FAR and LST showed a negative correlation in spring, autumn, and winter and a positive correlation in summer. However, the correlation increased with the increase of grid scale in spring, summer, and winter, but decreased in autumn.

Note: From left to right and from top to bottom, the order is the correlation between LST and USF in spring, summer, autumn, and winter.

3.3. Importance of USF indicator variables

Fig. 5 shows the relative importance of each USF indicator to the LST calculated by the XGBoost model. Differences in relative importance could be observed in different seasons and on different grid scales. Building morphology had the strongest importance to seasonal LST,

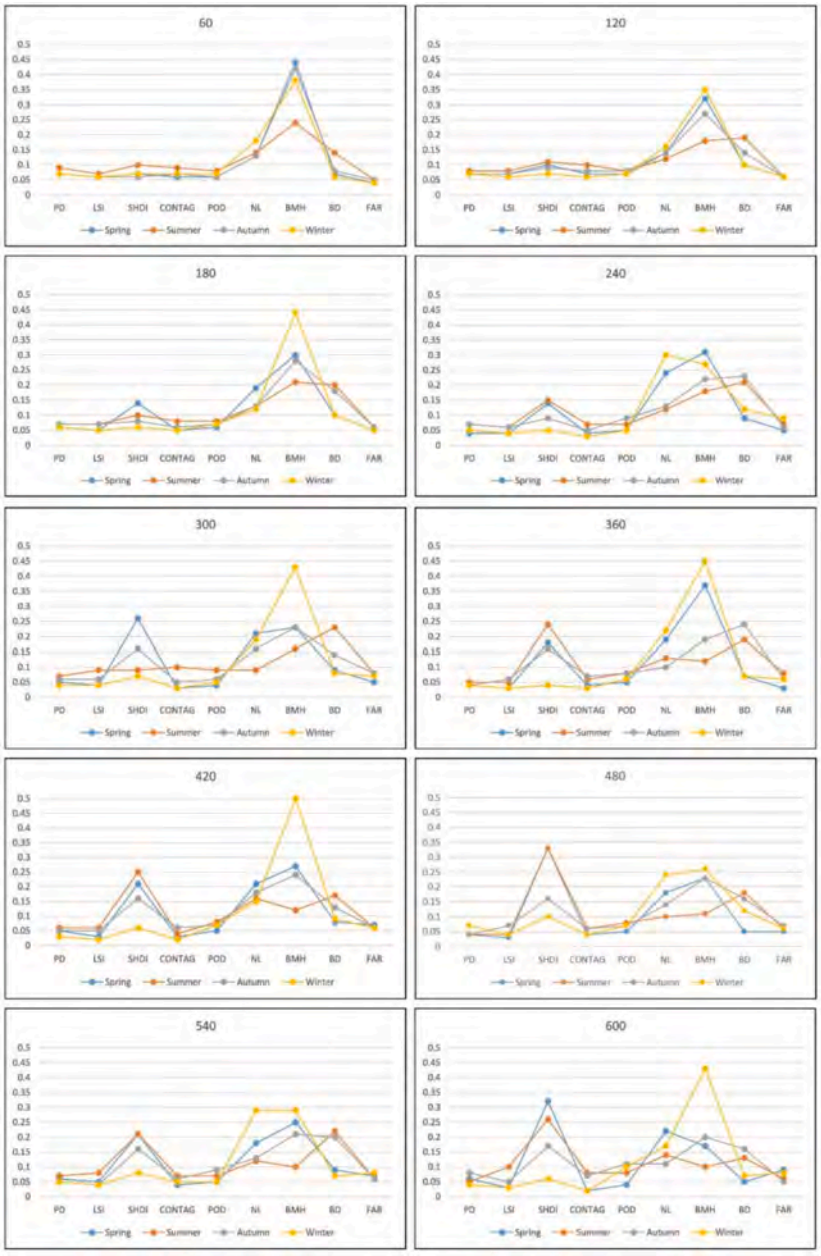

Fig. 5. Relative variable importance calculated by the XGBoost model.

followed by landscape pattern, and then social development. Specifically, BMH, NL and SHDI were the three most important variables for spring LST. The importance of SHDI has remained high from the from the 300 m grid scale and was strongest at the 480 m scale, whereas MAH was the most important variable at the 60 m and 360 m scales. The importance of the indicators in the summer and autumn LST showed a

Table 5
R^2 and MSE of the XGBoost model at different grid scales in the four seasons.

Grid Scale	R^2				MSE			
	Spring	Summer	Autumn	Winter	Spring	Summer	Autumn	Winter
60 m	0.64	0.61	0.62	0.63	1.43	1.68	1.26	0.69
120 m	0.50	0.49	0.48	0.46	1.81	2.04	1.54	0.97
180 m	0.48	0.48	0.47	0.46	1.72	2.06	1.41	0.89
240 m	0.49	0.47	0.45	0.46	1.82	2.12	1.43	0.93
300 m	0.51	0.43	0.42	0.47	1.50	2.01	1.32	0.76
360 m	0.48	0.48	0.47	0.50	1.52	1.83	1.10	0.64
420 m	0.55	0.48	0.43	0.51	1.33	1.81	1.21	0.65
480 m	0.50	0.43	0.36	0.51	1.34	1.77	1.08	0.64
540 m	0.58	0.50	0.51	0.56	1.05	1.40	0.84	0.57
600 m	0.60	0.54	0.52	0.61	1.06	1.30	0.80	0.47

similar pattern, and the top four were classified into BMH, BD, NL, and SHDI. The important indicators in winter were the same as in spring; however, in spring, the difference in importance between SHDI and NL was small, whereas in winter, the difference was great, with SHDI being much lower than NL.

This study used 10 grid scales (from 60 to 600 m, with a step size of 60 m) to establish XGBoost regression model to calculate the relationship between the corresponding USF index and LST, and explored the scale effect of this relationship. Furthermore, to provide useful reference for urban planning practice, this study selected the best grid scale of the XGBoost model according to the overall determination coefficient (R^2) and the mean square error (MSE) of the test data set as evaluation indicators of model performance. The experimental results of model R^2 and MSE are shown in Table 5.

The R^2 value in Table 5 decreases and then increases with increasing grid scale, whereas the MSE value increases and then decreases. Considering the performance of R^2 and MSE in different seasons and the area of the study area, 60 m is the appropriate size to study the relationship between USF and LST. At the 60 m grid scale, the R^2 of the four seasons is greater than 0.6, indicating that the contribution of the nine USF selected in this study to the seasonal LST is greater than 60%, showing USF plays an important role in influencing the LST of a city. At the 60 m grid scale, the highest contribution of USF to LST is building morphology. Three building morphology indicators effect more than 43% of LST, of which the largest impact is on spring and autumn LST (55%), and the smallest is in summer (43%). The second is the landscape pattern, and four landscape pattern indicators affect 26%–35% of LST. The last is social development, and the two social development indicators affect 19%–25% of LST.

4. Discussion

4.1. Effects of USF indicators on seasonal LST

A city is a complex ecosystem. USFs are a specific material form manifested by geographical entities; their type and layout significantly affect the accumulation and release of heat, leading to high local LST and results in a series of thermal environment problems that endanger the living environment and human thermal comfort (Lai et al., 2019; Zhao et al., 2018). Current research has paid more attention to single indicators, such as the structure of the road network, or remote sensing spectral index, when exploring the driving factors of LST (Yue et al., 2007; Zhang et al., 2017; Zullo et al., 2019). With the development of related research on USFs in the 3D and vertical directions, the influence of average building height, FAR, and building-related indicators on LST is being extensively studied (H. Lu et al., 2021). Although existing studies have covered most of the LST drivers, these studies have focused only on single LST explanatory variables, ignoring the multidimensionality of the variables (A. Guo et al., 2020a). Therefore, this study comprehensively selected nine explanatory variables, PD, LSI, SHDI, CONTAG, POD, NL, BMH, BD, and FAR, to describe the aspects of landscape, society, and architecture in USF.

Compared with previous studies, this study first explains the action form of various components of USF on seasonal LST. The main driving factors of LST vary with seasons, and the difference is most obvious in summer. The most significant factor affecting LST in spring, autumn and winter is MAH, and LST in summer is jointly affected by MAH, BD and SHDI. Building morphology is the most important indicator of the USF that affects seasonal LST, because buildings are the main content of urban construction during urbanization and are an important contributor to urban energy balance. Especially in winter, the weakening effect of MAH on LST is consistent with the scale, which may be due to buildings differing from natural vegetation and are insensitive to seasonal changes from spring to autumn. However, in winter, it is most likely that MAH has a significant cooling effect on LST due to the reduction of sunshine time and intensity, and the increase of shadow effect caused by the shielding of large walls (Theeuwes et al., 2014). Compared with building morphology, the ability of landscape pattern indicators to describe LST fluctuations is less. Although some studies have shown that increasing the area of greenery and water bodies can contribute to effectively mitigating the UHI effect (Cai et al., 2018; Cui et al., 2021); this study indicates that in the landscape pattern, except the abundance of land-use patches, the density, complexity and aggregation and diffusion of landscape patches have a limited impact on the seasonal LST. According to this study, social development is the least important factor influencing the economy. This means that social development parameters are not the dominant factors driving seasonal LST changes. This phenomenon may be explained by population activity, which is characterized by population density, and social development, which is characterized by nighttime lighting, having somewhat homogeneous characteristics at the smaller grid scales.

4.2. Scale effects of USF indicators on LST

To explore the driving factors and the mechanism of the UHI effect and, thus, to explore the mitigation of the urban heat problem and achieve the goal of optimizing the urban thermal environment, studies have previously been conducted on the influencing factors of LST on different scales. On different research scales, certain differences have been observed in the important factors that influence LST in the studied areas. On an urban scale such as in Suzhou, the land cover index is the dominant factor in LST, but spatial proximity and location also greatly influence its distribution (Feng et al., 2019). And at the community scale, the LST in Ganjingzi District of Dalian is most affected by land-use type, landscape index, and remote sensing index, followed by nighttime illumination and socioeconomic characteristics, whereas spatial form is the least influential index (A. Guo et al., 2020b). Furthermore, when the number of selected indicators changes, the appropriate spatial scale may also change (Dai et al., 2018).

This study explains the scale effect between USF indicators and seasonal LST second. Our results show that the impact of various USF indicators on LST is scale-dependent, which is mainly reflected in the following two aspects. On the one hand, with the change in grid scale, the influence of some indicators on LST increased or decreased significantly. For example, the influence of SHDI on the autumn LST increased from the grid scale of 300 m, and the influence of BMH on the summer LST decreased from the grid scale of 360 m. On the other hand, some indicators are important for LST at certain specific scales, such as SHDI for summer LST at the 480 m scale.

This study also found the appropriate scale to study the relationship between USF and LST. This study discusses the influence of USF on LST at different grid scales. The specific method was to aggregate and average LST in the grid cell and calculate different USF indicators in the grid. In the experiment, 10 grid scales from 60 to 600 m were discussed. The overall trend was that R^2 value decreased first and then increased with the increase of grid, whereas MSE was on the contrary. The 60 m grid has the highest R^2. The grid size of 30 m is too small, resulting in too many grids. However, due to insufficient memory of analysis software, spatial statistical analysis cannot be performed. Therefore, considering the accuracy of the model, the size of the study area and the number of grids, 60 m was determined as the appropriate grid scale for studying the relationship between USF and LST in this study, which also follows the research of Song and other scholars (Song et al., 2014).

4.3. Implications for urban planning and management

In this study, we explored the relationship between LST and various USF indicators and ranked the relative importance of each indicator. Therefore, the funding of this study can help urban planners and planning departments to better understand the impact mechanism of USF on the urban thermal environment to provide strategic guidance for ecological environment construction and formulation, implementation,

and management of urban planning strategies.

The XGBoost model provides a realistic and effective method to determine the relative contribution of USF to LST, thus revealing the influencing factors of seasonal LST. Our study has determined that building morphology indicators are the most important factor influencing LST. Among them, MAH is significantly negatively correlated with the LST in all four seasons. Because the NL is also negatively correlated with LST, and the regional light intensity of high-rise buildings is relatively high, the shadow of high-rise buildings has a certain effect on reducing LST. However, the purpose of mitigating the UHI effect cannot be achieved by building the number of new high-rise buildings, because BD is positively related to LST. Therefore, urban planners should try to reduce BD while building high-rise structures to mitigate the urban thermal environment by increasing the shaded area and improving local ventilation.

This study determined that the landscape pattern has less influence on LST than the building morphology. The distribution densities, shapes, and degrees of aggregation and spreading of different types of landscape patches have a relatively weak influence on LST. However, other studies have shown that increasing the area of greenery and water bodies can effectively improve the UHI effect (C. Yang et al., 2017; Yu et al., 2020). Therefore, the impact of green landscapes, including ground cover, shrubs, and trees on LST is reflected in the increase in their number and area, rather than their specific distribution. A relatively pleasant habitat should have high-rise low-density buildings and plenty of greenery and water bodies (Ren et al., 2023).

Based on the research on the relative contribution of different urban form indicators to the seasonal LST, the following planning suggestions on improving the thermal environment of the urban center are proposed: (1) More attention should be paid to the building morphology indicators rather than the landscape pattern indicators and social development indicators, because the building morphology indicators have a higher relative contribution to seasonal LST. (2) Blocks with high-rise low-density buildings will be the best to change the regional thermal environment. However, due to the limited construction land, it is necessary to avoid the gathering of multiple low-density high-rise building blocks and increase the area of water and green space to adjust the regional thermal environment. (3) Besides the perspective of urban morphology in this study, building materials, vertical greening and other measures can also be considered (Zhang & He, 2021).

4.4. Limitations

In this study, the effects of USF on LST were explored in four seasons at 10 grid scales. Although using the RTE method to retrieve LST with Landsat8 images has high accuracy, due to the limitation of cloud cover and the satellite revisit period, only one-scene image was selected in each season to explore the relationship between USFs and LST, without considering the trend of variation of LST in terms of seasons, months, and days. Therefore, future studies should use multi-sensor and multi-temporal remote sensing imagery to provide more accurate time series data for LST (Desai et al., 2021; Gomez-Martinez et al., 2021). Second, inconsistencies exist in the spatial scale of the experimental data, especially the spatial resolution of the VIIRS-NPP nighttime lighting data is low. Although reclassification was used to unify the data in the process, it is still necessary to apply high-resolution multi-source data to describe the USFs more accurately (Chang et al., 2020). Finally, the description of USFs still needs to be further improved. Due to the unavailability of datasets, this study selected only nine indicators of three aspects: landscape pattern, architectural form, and socioeconomics. Although USFs have been described in multiple dimensions to some extent, this definition cannot completely describe the morphological characteristics of buildings and urban green landscapes. For example, vertical information of buildings and 3D structure of trees may be easily overlooked (Chen et al., 2021; Guo et al., 2021). Moreover, USFs may vary with different geographical settings and climatic backgrounds, thus it is necessary to conduct experiments across cities in representative locations.

5. Conclusion

In this study, we investigated the influence of the USF on seasonal LST at different grid scales. To achieve this, we took the main area of Xi'an City as the study area and selected four seasons of daytime cloud-free Landsat8 remote sensing imagery; we then retrieved LST using the high-precision RTE method to explore the spatial distribution characteristics of LST in the study area during all seasons. At the same time, we used multiple data sources and selected nine indicators to quantitatively characterize the USF from three perspectives: landscape pattern, building morphology, and social development. The magnitude of impact for each indicator on LST was assessed using the XGBoost model, which has better accuracy than support vector machines, random forest, and deep learning neural networks (Stojić et al., 2019). The main findings of this study are as follows:

(1) The remote sensing retrieval results show that the spatial distribution pattern of LST in spring and autumn is similar, but the overall LST in winter is significantly lower.. Large areas with high temperature are mainly distributed in the southwest of Weiyang, the southeast of Baqiao, and the west of Yanta districts in spring and winter, whereaas in the Lianhu, Xincheng, and Beilin district in the summer and autumn. Furthermore, low LST is mainly distributed in the water body and near the park in the north and south of the central part of the study area, which is less affected by the season.

(2) Pearson correlation analysis shows that the relationship between LST and USF indicators with seasons. MAH is a seasonal stable factor with cooling effect. The relationship between PD, LSI, SHDI, CONTAG, POD, FAR, and LST varies with seasons. The correlation between BD and LST is the most complex. Spring and autumn are bounded by a 120 m grid. When the grid scale is less than 120 m, BD is positively correlated with LST; however, it is negatively correlated. BD and LST were positively correlated in summer and autumn. In addition, the correlation between LST and each indicator in autumn was much lower than that in the other three seasons, and the correlation between landscape pattern indicators and LST was extremely low.

(3) The order of importance of indicators that affect seasonal LST was: building morphology > landscape pattern > social development. Specifically, the three most important indicators for LST in spring and winter were BMH, NL, and SHDI, and their importance changed according to different scales. The importance of indicators of LST in summer and autumn showed a similar pattern, and the top four indicators were BMH, BD, NL and SHDI.

(4) The appropriate size to study the relationship between USF and seasonal LST is 60 m. The highest contribution of USF to LST is building morphology, three indicators affect 43%–55% of LST. The second is the landscape pattern, and the four indicators affect 26%–35% of LST. The last is social development, and the two indicators affect 19%–25% of LST.

Declaration of Competing Interest

The authors declare that they have no known competing financial interests or personal relationships that could have appeared to influence the work reported in this paper.

Data availability

Data will be made available on request.

References

Aghamohammadi, N., Fong, C. S., Idrus, M. H. M., Ramakreshnan, L., & Sulaiman, N. M. (2021). Environmental heat-related health symptoms among community in a tropical city. *Science of The Total Environment, 782*, Article 146611. https://doi.org/10.1016/j.scitotenv.2021.146611

Barsi, J. A., Schott, J. R., Palluconi, F. D., Helder, D. L., Hook, S. J., Markham, B. L., Chander, G., & O'Donnell, E. M. (2003). Landsat TM and ETM+ thermal band calibration. *Canadian Journal of Remote Sensing, 29*, 141–153. https://doi.org/10.5589/m02-087

Cai, Z., Han, G., & Chen, M. (2018). Do water bodies play an important role in the relationship between urban form and land surface temperature? *Sustainable Cities and Society, 39*, 487–498. https://doi.org/10.1016/j.scs.2018.02.033

Chang, C.-C., & Lin, C.-J. (2011). LIBSVM: A library for support vector machines. *ACM Trans. Intell. Syst. Technol., 2*. https://doi.org/10.1145/1961189.1961199, 27:1-27:27.

Chang, S., Wang, Z., Mao, D., Guan, K., Jia, M., & Chen, C. (2020). Mapping the Essential Urban Land Use in Changchun by Applying Random Forest and Multi-Source Geospatial Data. *Remote Sensing, 12*, 2488. https://doi.org/10.3390/rs12152488

Chen, J., Zhan, W., Jin, S., Han, W., Du, P., Xia, J., Lai, J., Li, J., Liu, Z., Li, L., Huang, F., & Ding, H. (2021). Separate and combined impacts of building and tree on urban thermal environment from two- and three-dimensional perspectives. *Building and Environment, 194*, Article 107650. https://doi.org/10.1016/j.buildenv.2021.107650

Chen, T., & Guestrin, C. (2016). XGBoost: A Scalable Tree Boosting System. In *The 22nd ACM SIGKDD International Conference*.

Chun, B., & Guldmann, J.-M. (2014). Spatial statistical analysis and simulation of the urban heat island in high-density central cities. *Landscape and Urban Planning, 125*, 76–88. https://doi.org/10.1016/j.landurbplan.2014.01.016

Cui, F., Hamdi, R., Yuan, X., He, H., Yang, T., Kuang, W., Termonia, P., & De Maeyer, P. (2021). Quantifying the response of surface urban heat island to urban greening in global north megacities. *Science of The Total Environment, 801*, Article 149553. https://doi.org/10.1016/j.scitotenv.2021.149553

Dai, Z., Guldmann, J.-M., & Hu, Y. (2018). Spatial regression models of park and land-use impacts on the urban heat island in central Beijing. *Science of The Total Environment, 626*, 1136–1147. https://doi.org/10.1016/j.scitotenv.2018.01.165

Dan, Y., Li, H., Jiang, S., Yang, Z., & Peng, J. (2022). Changing coordination between urban area with high temperature and multiple landscapes in Wuhan City. *China. Sustainable Cities and Society, 78*, Article 103586. https://doi.org/10.1016/j.scs.2021.103586

Desai, A. R., Khan, A. M., Zheng, T., Paleri, S., Butterworth, B., Lee, T. R., Fisher, J. B., Hulley, G., Kleynhans, T., Gerace, A., Townsend, P. A., Stoy, P., & Metzger, S. (2021). Multi-Sensor Approach for High Space and Time Resolution Land Surface Temperature. *Earth and Space Science, 8*, Article e2021EA001842. https://doi.org/10.1029/2021EA001842

Equere, V., Mirzaei, P. A., & Riffat, S. (2020). Definition of a new morphological parameter to improve prediction of urban heat island. *Sustainable Cities and Society, 56*, Article 102021. https://doi.org/10.1016/j.scs.2020.102021

Esch, T., Marconcini, M., Marmanis, D., Zeidler, J., Elsayed, S., Metz, A., Müller, A., & Dech, S. (2014). Dimensioning urbanization – An advanced procedure for characterizing human settlement properties and patterns using spatial network analysis. *Applied Geography, 55*, 212–228. https://doi.org/10.1016/j.apgeog.2014.09.009

Estoque, R. C., Murayama, Y., & Myint, S. W. (2017). Effects of landscape composition and pattern on land surface temperature: An urban heat island study in the megacities of Southeast Asia. *Science of The Total Environment, 577*, 349–359. https://doi.org/10.1016/j.scitotenv.2016.10.195

Fan, J., Wang, X., Wu, L., Zhou, H., Zhang, F., Yu, X., Lu, X., & Xiang, Y. (2018). Comparison of Support Vector Machine and Extreme Gradient Boosting for predicting daily global solar radiation using temperature and precipitation in humid subtropical climates: A case study in China. *Energy Conversion and Management, 164*, 102–111. https://doi.org/10.1016/j.enconman.2018.02.087

Feng, Y., Gao, C., Tong, X., Chen, S., Lei, Z., & Wang, J. (2019). Spatial Patterns of Land Surface Temperature and Their Influencing Factors: A Case Study in Suzhou. *China. Remote Sensing, 11*, 182. https://doi.org/10.3390/rs11020182

Fotheringham, A. S., Yang, W., & Kang, W. (2017). Multiscale Geographically Weighted Regression (MGWR). *Annals of the American Association of Geographers, 107*, 1247–1265. https://doi.org/10.1080/24694452.2017.1352480

Gao, S., Zhan, Q., Yang, C., & Liu, H. (2020). The Diversified Impacts of Urban Morphology on Land Surface Temperature among Urban Functional Zones. *Int J Environ Res Public Health, 17*, E9578. https://doi.org/10.3390/ijerph17249578

Gomez-Martinez, F., de Beurs, K. M., Koch, J., & Widener, J. (2021). Multi-Temporal Land Surface Temperature and Vegetation Greenness in Urban Green Spaces of Puebla. *Mexico. Land, 10*, 155. https://doi.org/10.3390/land10020155

Guo, A., Yang, J., Sun, W., Xiao, X., Xia Cecilia, J., Jin, C., & Li, X. (2020a). Impact of urban morphology and landscape characteristics on spatiotemporal heterogeneity of land surface temperature. *Sustainable Cities and Society, 63*, Article 102443. https://doi.org/10.1016/j.scs.2020.102443

Guo, A., Yang, J., Xiao, X., Xia (Cecilia), J., Jin, C., & Li, X. (2020b). Influences of urban spatial form on urban heat island effects at the community level in China. *Sustainable Cities and Society, 53*, Article 101972. https://doi.org/10.1016/j.scs.2019.101972

Guo, F., Wu, Q., & Schlink, U. (2021). 3D building configuration as the driver of diurnal and nocturnal land surface temperatures: Application in Beijing's old city. *Building and Environment, 206*, Article 108354. https://doi.org/10.1016/j.buildenv.2021.108354

Guo, G., Wu, Z., Xiao, R., Chen, Y., Liu, X., & Zhang, X. (2015). Impacts of urban biophysical composition on land surface temperature in urban heat island clusters. *Landscape and Urban Planning, 135*, 1–10. https://doi.org/10.1016/j.landurbplan.2014.11.007

Guo, J., Han, G., Xie, Y., Cai, Z., & Zhao, Y. (2020). Exploring the relationships between urban spatial form factors and land surface temperature in mountainous area: A case study in Chongqing city. *China. Sustainable Cities and Society, 61*, Article 102286. https://doi.org/10.1016/j.scs.2020.102286

Howard, L., 2012. The climate of London, deduced from meteorological observations. The climate of London, deduced from meteorological observations.

Huang, X., Wang, H., Shan, L., & Xiao, F. (2021). Constructing and optimizing urban ecological network in the context of rapid urbanization for improving landscape connectivity. *Ecological Indicators, 132*, Article 108319. https://doi.org/10.1016/j.ecolind.2021.108319

He, B., Wang, J., Zhu, J., & Qi, J. (2022). Beating the urban heat: Situation, background, impacts and the way forward in China. *Renewable and Sustainable Energy Reviews, 161*, 112350. https://doi.org/10.1016/j.rser.2022.112350

He, B., Zhao, D., Dong, X., Zhao, Z., Li, L., Duo, L., & Li, J. (2022). Will individuals visit hospitals when suffering heat-related illnesses? *Yes, but…. Building and Environment, 208*, 108587. https://doi.org/10.1016/j.buildenv.2021.108587

Huang, X., & Wang, Y. (2019). Investigating the effects of 3D urban morphology on the surface urban heat island effect in urban functional zones by using high-resolution remote sensing data: A case study of Wuhan, Central China. *ISPRS Journal of Photogrammetry and Remote Sensing, 152*, 119–131. https://doi.org/10.1016/j.isprsjprs.2019.04.010

Kim, J.-H., Gu, D., Sohn, W., Kil, S.-H., Kim, H., & Lee, D.-K. (2016). Neighborhood Landscape Spatial Patterns and Land Surface Temperature: An Empirical Study on Single-Family Residential Areas in Austin, Texas. *Int J Environ Res Public Health, 13*, E880. https://doi.org/10.3390/ijerph13090880

Lai, D., Liu, W., Gan, T., Liu, K., & Chen, Q. (2019). A review of mitigating strategies to improve the thermal environment and thermal comfort in urban outdoor spaces. *Science of The Total Environment, 661*, 337–353. https://doi.org/10.1016/j.scitotenv.2019.01.062

Li, G., & Li, Y. (2021). Optimization spatial pattern method for vegetation landscape in bay based on. *AHP. Microprocessors and Microsystems, 83*, Article 104041. https://doi.org/10.1016/j.micpro.2021.104041

Li, H., Li, Y., Wang, T., Wang, Z., Gao, M., & Shen, H. (2021). Quantifying 3D building form effects on urban land surface temperature and modeling seasonal correlation patterns. *Building and Environment, 204*, Article 108132. https://doi.org/10.1016/j.buildenv.2021.108132

Li, S., Zhao, Z., Miaomiao, X., & Wang, Y. (2010). Investigating spatial non-stationary and scale-dependent relationships between urban surface temperature and environmental factors using geographically weighted regression. *Environmental Modelling & Software, 25*, 1789–1800. https://doi.org/10.1016/j.envsoft.2010.06.011

Li, W., Cao, Q., Lang, K., & Wu, J. (2017). Linking potential heat source and sink to urban heat island: Heterogeneous effects of landscape pattern on land surface temperature. *Science of The Total Environment, 586*, 457–465. https://doi.org/10.1016/j.scitotenv.2017.01.191

Li, X., Zhou, Y., Asrar, G.R., Imhoff, M., Li, Xuecao, 2017. The surface urban heat island response to urban expansion: A panel analysis for the conterminous United States. Science of The Total Environment 605–606, 426–435. https://doi.org/10.1016/j.scitotenv.2017.06.229.

Li, Y., Schubert, S., Kropp, J. P., & Rybski, D. (2020). On the influence of density and morphology on the Urban Heat Island intensity. *Nat Commun, 11*, 2647. https://doi.org/10.1038/s41467-020-16461-9

Li, Z., & Hu, D. (2022). Exploring the relationship between the 2D/3D architectural morphology and urban land surface temperature based on a boosted regression tree: A case study of Beijing. *China. Sustainable Cities and Society, 78*, Article 103392. https://doi.org/10.1016/j.scs.2021.103392

Liang, Z., Wu, S., Wang, Y., Wei, F., Huang, J., Shen, J., & Li, S. (2020). The relationship between urban form and heat island intensity along the urban development gradients. *Science of The Total Environment, 708*, Article 135011. https://doi.org/10.1016/j.scitotenv.2019.135011

Liu, H., Huang, B., Zhan, Q., Gao, S., Li, R., & Fan, Z. (2021). The influence of urban form on surface urban heat island and its planning implications: Evidence from 1288 urban clusters in China. *Sustainable Cities and Society, 71*, Article 102987. https://doi.org/10.1016/j.scs.2021.102987

Liu, H., Zhan, Q., Gao, S., Yang, C., 2019. Seasonal Variation of the Spatially Non-Stationary Association Between Land Surface Temperature and Urban Landscape. Remote Sensing 11, 1016. https://doi.org/10.3390/rs11091016.

Liu, Y., Arp, H. P. H., Song, X., & Song, Y. (2017). Research on the relationship between urban form and urban smog in China. *Environment and Planning B: Urban Analytics and City Science, 44*, 328–342. https://doi.org/10.1177/0265813515624687

Lu, H., Li, F., Yang, G., & Sun, W. (2021). Multi-scale impacts of 2D/3D urban building pattern in intra-annual thermal environment of Hangzhou. *China. International Journal of Applied Earth Observation and Geoinformation, 104*, Article 102558. https://doi.org/10.1016/j.jag.2021.102558

Lu, Y., Yue, W., Liu, Y., & Huang, Y. (2021). Investigating the spatiotemporal non-stationary relationships between urban spatial form and land surface temperature: A case study of Wuhan. *China. Sustainable Cities and Society, 72*, Article 103070. https://doi.org/10.1016/j.scs.2021.103070

Mandal, J., Patel, P. P., & Samanta, S. (2021). Examining the expansion of Urban Heat Island effect in the Kolkata Metropolitan Area and its vicinity using multi-temporal MODIS satellite data. *Advances in Space Research*. https://doi.org/10.1016/j.asr.2021.11.040

Morabito, M., Crisci, A., Messeri, A., Orlandini, S., Raschi, A., Maracchi, G., & Munafò, M. (2016). The impact of built-up surfaces on land surface temperatures in Italian urban

areas. *Science of The Total Environment, 551–552*, 317–326. https://doi.org/10.1016/j.scitotenv.2016.02.029

Oke, T. R., Mills, G., Christen, A., & Voogt, J. A. (2017). *Urban Climates, Cambridge Books*. Cambridge University Press.

Qu, B., Zhu, W., Jia, S., & Lv, A. (2015). Spatio-Temporal Changes in Vegetation Activity and Its Driving Factors during the Growing Season in China from 1982 to 2011. *Remote Sensing, 7*, 13729–13752. https://doi.org/10.3390/rs71013729

Sharifi, A. (2019). Urban form resilience: A meso-scale analysis. *Cities, 93*, 238–252. https://doi.org/10.1016/j.cities.2019.05.010

Shi, K., Wang, H., Yang, Q., Wang, L., Sun, X., & Li, Y. (2019). Exploring the relationships between urban forms and fine particulate (PM2.5) concentration in China: A multi-perspective study. *Journal of Cleaner Production, 231*, 990–1004. https://doi.org/10.1016/j.jclepro.2019.05.317

Sobrino, J. A., Jiménez-Muñoz, J. C., & Paolini, L. (2004). Land surface temperature retrieval from LANDSAT TM 5. *Remote Sensing of Environment, 90*, 434–440. https://doi.org/10.1016/j.rse.2004.02.003

Sobstyl, J., Emig, T., Abdolhosseini Qomi, M. J., Ulm, F.-J., & Pellenq, R. (2018). Role of City Texture in Urban Heat Islands at Nighttime. *Physical Review Letters, 120*. https://doi.org/10.1103/PhysRevLett.120.108701

Song, J., Du, S., Feng, X., & Guo, L. (2014). The relationships between landscape compositions and land surface temperature: Quantifying their resolution sensitivity with spatial regression models. *Landscape and Urban Planning, 123*, 145–157. https://doi.org/10.1016/j.landurbplan.2013.11.014

Stojić, A., Stanić, N., Vuković, G., Stanišić, S., Perišić, M., Šoštarić, A., & Lazić, L. (2019). Explainable extreme gradient boosting tree-based prediction of toluene, ethylbenzene and xylene wet deposition. *Science of The Total Environment, 653*, 140–147. https://doi.org/10.1016/j.scitotenv.2018.10.368

Stone, B., Vargo, J., & Habeeb, D. (2012). Managing climate change in cities: Will climate action plans work? *Landscape and Urban Planning, 107*, 263–271. https://doi.org/10.1016/j.landurbplan.2012.05.014

Sun, F., Liu, M., Wang, Y., Wang, H., & Che, Y. (2020). The effects of 3D architectural patterns on the urban surface temperature at a neighborhood scale: Relative contributions and marginal effects. *Journal of Cleaner Production, 258*, Article 120706. https://doi.org/10.1016/j.jclepro.2020.120706

Sun, Y., Gao, C., Li, J., Wang, R., & Liu, J. (2019a). Quantifying the Effects of Urban Form on Land Surface Temperature in Subtropical High-Density Urban Areas Using Machine Learning. *Remote Sensing, 11*, 959. https://doi.org/10.3390/rs11080959

Sun, Y., Gao, C., Li, J., Wang, R., & Liu, J. (2019b). Evaluating urban heat island intensity and its associated determinants of towns and cities continuum in the Yangtze River Delta Urban Agglomerations. *Sustainable Cities and Society, 50*, Article 101659. https://doi.org/10.1016/j.scs.2019.101659

Taleghani, M., Kleerekoper, L., Tenpierik, M., & van den Dobbelsteen, A. (2015). Outdoor thermal comfort within five different urban forms in the Netherlands. *Building and Environment, Special Issue: Climate adaptation in cities, 83*, 65–78. https://doi.org/10.1016/j.buildenv.2014.03.014

Taubenböck, H., Wurm, M., Geiß, C., Dech, S., & Siedentop, S. (2019). Urbanization between compactness and dispersion: designing a spatial model for measuring 2D binary settlement landscape configurations. *International Journal of Digital Earth, 12*, 679–698. https://doi.org/10.1080/17538947.2018.1474957

Theeuwes, N. E., Steeneveld, G. J., Ronda, R. J., Heusinkveld, B. G., van Hove, L. W. A., & Holtslag, A.a. M. (2014). Seasonal dependence of the urban heat island on the street canyon aspect ratio. *Quarterly Journal of the Royal Meteorological Society, 140*, 2197–2210. https://doi.org/10.1002/qj.2289

Tsai, Y.-H. (2005). Quantifying Urban Form: Compactness versus "Sprawl. *Urban Studies, 42*, 141–161. https://doi.org/10.1080/0042098042000309748

Wang, Y., Sheng, S., & Xiao, H. (2021). The cooling effect of hybrid land-use patterns and their marginal effects at the neighborhood scale. *Urban Forestry & Urban Greening, 59*, Article 127015. https://doi.org/10.1016/j.ufug.2021.127015

Yang, C., He, X., Wang, R., Yan, F., Yu, L., Bu, K., Yang, J., Chang, L., & Zhang, S. (2017). The Effect of Urban Green Spaces on the Urban Thermal Environment and Its Seasonal Variations. *Forests, 8*, 153. https://doi.org/10.3390/f8050153

Yang, J., Ren, J., Sun, D., Xiao, X., Xia, J, (Cecilia), Jin, C., & Li, X. (2021a). Understanding land surface temperature impact factors based on local climate zones. *Sustainable Cities and Society, 69*, Article 102818. https://doi.org/10.1016/j.scs.2021.102818

Yang, J., Sun, J., Ge, Q., & Li, X. (2017). Assessing the impacts of urbanization-associated green space on urban land surface temperature: A case study of Dalian. *China. Urban Forestry & Urban Greening, 22*, 1–10. https://doi.org/10.1016/j.ufug.2017.01.002

Yang, J., Yang, Y., Sun, D., Jin, C., & Xiao, X. (2021b). Influence of urban morphological characteristics on thermal environment. *Sustainable Cities and Society, 72*, Article 103045. https://doi.org/10.1016/j.scs.2021.103045

Yang, J., Zhan, Y., Xiao, X., Xia, J.C., Sun, W., Li, X., 2020. Investigating the diversity of land surface temperature characteristics in different scale cities based on local climate zones. Urban Climate 34, 100700. https://doi.org/10.1016/j.uclim.2020.100700.

Yang, X., & Jin, W. (2010). GIS-based spatial regression and prediction of water quality in river networks: A case study in Iowa. *Journal of Environmental Management, 91*, 1943–1951. https://doi.org/10.1016/j.jenvman.2010.04.011

Yu, X., Guo, X., & Wu, Z. (2014). Land Surface Temperature Retrieval from Landsat 8 TIRS—Comparison between Radiative Transfer Equation-Based Method, Split Window Algorithm and Single Channel Method. *Remote Sensing, 6*, 9829–9852. https://doi.org/10.3390/rs6109829

Yu, Z., Yang, G., Zuo, S., Jørgensen, G., Koga, M., Vejre, H., 2020. Critical review on the cooling effect of urban blue-green space: A threshold-size perspective. Urban Forestry & Urban Greening 49, 126630. https://doi.org/10.1016/j.ufug.2020.126630.

Yue, W., Xu, J., Tan, W., & Xu, L. (2007). The relationship between land surface temperature and NDVI with remote sensing: application to Shanghai Landsat 7 ETM + data. *International Journal of Remote Sensing, 28*, 3205–3226. https://doi.org/10.1080/01431160500306906

Zhang, G., & He, B. (2021). Towards green roof implementation: Drivers, motivations, barriers and recommendations. *Urban forestry & urban greening, 58*, 126992. https://doi.org/10.1016/j.ufug.2021.126992

Zhang, X., & Sun, Y. (2019). Investigating institutional integration in the contexts of Chinese city-regionalization: Evidence from Shenzhen–Dongguan–Huizhou. *Land Use Policy, 88*, Article 104170. https://doi.org/10.1016/j.landusepol.2019.104170

Zhang, Y., Murray, A. T., & Turner, B. L. (2017). Optimizing green space locations to reduce daytime and nighttime urban heat island effects in Phoenix. *Arizona. Landscape and Urban Planning, 165*, 162–171. https://doi.org/10.1016/j.landurbplan.2017.04.009

Zhao, M., Cai, H., Qiao, Z., & Xu, X. (2016). Influence of urban expansion on the urban heat island effect in Shanghai. *International Journal of Geographical Information Science, 30*, 2421–2441. https://doi.org/10.1080/13658816.2016.1178389

Zhao, Q., Sailor, D. J., & Wentz, E. A. (2018). Impact of tree locations and arrangements on outdoor microclimates and human thermal comfort in an urban residential environment. *Urban Forestry & Urban Greening, 32*, 81–91. https://doi.org/10.1016/j.ufug.2018.03.022

Zhou, B., Rybski, D., & Kropp, J. P. (2017). The role of city size and urban form in the surface urban heat island. *Sci Rep, 7*, 4791. https://doi.org/10.1038/s41598-017-04242-2

Zhou, X., & Chen, H. (2018). Impact of urbanization-related land use land cover changes and urban morphology changes on the urban heat island phenomenon. *Science of The Total Environment, 635*, 1467–1476. https://doi.org/10.1016/j.scitotenv.2018.04.091

Zullo, F., Fazio, G., Romano, B., Marucci, A., & Fiorini, L. (2019). Effects of urban growth spatial pattern (UGSP) on the land surface temperature (LST): A study in the Po Valley (Italy). *Science of The Total Environment, 650*, 1740–1751. https://doi.org/10.1016/j.scitotenv.2018.09.331

Ren, J., Yang, J., Wu, F., Sun, W., Xiao, X., & Xia, J.(C.) (2023). Regional thermal environment changes: Integration of satellite data and land use/land cover. ISCIENCE, doi: 10.1016/j.isci.2022.105820.